International Journal of Biological Macromolecules 209 (2022) 1234–1247

Contents lists available at ScienceDirect

International Journal of Biological Macromolecules

journal homepage: www.elsevier.com/locate/ijbiomac

Synthesis and characterization of chitosan-vermiculite-lignin ternary composite as an adsorbent for effective removal of uranyl ions from aqueous solution: Experimental and theoretical analyses

Zeynep Mine Şenol [a], Savaş Kaya [b], Selçuk Şimşek [b,*], K.P. Katin [c], Ali Özer [d], Riadh Marzouki [e,f]

[a] Sivas Cumhuriyet University, Zara Vocational School, Department of Food Technology, 58140 Sivas, Turkey
[b] Sivas Cumhuriyet University, Faculty of Science, Department of Chemistry, 58140 Sivas, Turkey
[c] Institute of Nanoengineering in Electronics, Spintronics and Photonics, National Research Nuclear University "MEPhI", Kashirskoe Shosse 31, Moscow 115409, Russia
[d] Sivas Cumhuriyet University, Eng. Fac., Metallurgical and Materials Eng. Dept., 58140 Sivas, TÜRKİYE
[e] Chemistry Department, College of Science, King Khalid University, Abha 61413, Saudi Arabia
[f] Laboratory of Materials, Crystallochemistry and Applied Thermodynamics, Faculty of Sciences of Tunis, University of Tunis El Manar, Tunisia

ARTICLE INFO

Keywords:
Chitosan
Vermiculite
Lignin
Ternary composite
Uranyl
Adsorption
DFT calculations

ABSTRACT

Chitosan (Ch), vermiculite (V) and lignin (L) were used as the components of a natural composite adsorbent (Ch-VL) for the removal of the UO_2^{2+} ions in aqueous solutions. During the study, we recorded and analyzed the initial UO_2^{2+} ion concentration, initial pH, contact time, temperature, and recovery. The recycling performance of the Ch-VL composite was assessed by three sequential adsorption/desorption experiments. Adsorption performance of the Ch-VL composite for UO_2^{2+} ions was 600 mg L^{-1} at pH 4.5 and temperature of 25 °C. Thermodynamic findings, ΔH^0:28.1 kJ mol^{-1}, and ΔG^0:−14.1 kJ mol^{-1} showed that adsorption behavior was endothermic and spontaneous. Its maximum adsorption capacity was 0.322 mol kg^{-1}, obtained from the Langmuir isotherm model. The adsorption kinetics indicated that it followed the pseudo-second-order and intraparticle diffusion rate kinetics. The adsorption thermodynamic shown indicated that the UO_2^{2+} ion adsorption was both spontaneous and endothermic. The adsorption process was enlightened by FT-IR and SEM-EDX analyses. The study suggested a simple and cost-effective approach for the removal of toxic UO_2^{2+} ions from wastewater. To highlight the adsorption mechanism, DFT calculations were performed. Theoretical results are in good agreement with experimental observations.

1. Introduction

Today, the increasing need for energy with increasing industrialization and the dependence on fossil fuels used have led to an increase in environmental pollution [1]. Alternative energy sources are of great importance in preventing environmental pollution [2]. Especially nuclear energy stands out among alternative energy sources. However, with nuclear energy, both the need for raw materials and the removal of radioactive waste from the environment have emerged as a new problem. Uranium is the main ingredient of nuclear energy [3]. However, its limited resources make it one of the research areas for its recovery in environments with lower concentrations such as seawater [4]. Recycling uranium is important for human health as well as removing it from wastewater. Because if uranium is taken into the body, its toxic effect on various organs negatively affects human health and can lead to death. From these two perspectives, usable, practical and economical ways to both recover and remove uranium open up new areas of research. The type in which uranium is found in an aqueous solution is the uranium hexavalent ion [5]. Some effective versatile low-cost adsorbents for removing uranyl ions from waters were introduced in the literature. Hamza et al. analyzed the performance of silica beads functionalized with urea- or thiourea-based polymers for the recovery U(VI) and Th (IV). The authors noted that U(VI) and Th (IV) maximum sorption capacities are 1–1.2 mmol g^{-1} at pH 5 [6]. Another comprehensive paper investigated the design of an effective adsorbent obtained with phosphorylation of guar gum combined with its association to chitosan for the removal of U(VI) from acidic solution [7]. Guibal grafted the magnetic chitosan micro-particles with amine and dithizone. In this study, it was noted that uranyl sorption highly increases with the functionalization of diethylenetriamine amine [8]. Guibal and coworkers showed that

* Corresponding author.
E-mail address: simsek@cumhuriyet.edu.tr (S. Şimşek).

https://doi.org/10.1016/j.ijbiomac.2022.04.128
Received 26 February 2022; Received in revised form 8 April 2022; Accepted 17 April 2022
Available online 21 April 2022

Table 1
Experimental conditions for adsorption process.

Experimental conditions					
Aim of experiment	Solution pH	Initial UO_2^{2+} conc. (mg L^{-1})	Adsorbent dosage (mg)	Contact time (min)	Temperature (°C)
Effect of pH	1.0–7.0	600	100	1440	25
Effect of concentration	4.5	50–1000	100	1440	25
Effect of time	4.5	600	300	2–1440	25
Effect of adsorbent dosage	4.5	600	10, 30, 50, 100, 200	1440	25
Effect of temperature	4.5	600	100	1440	5, 25, 40
Recovery	4.5	600	100	1440	25

tetraethylenepentamine modified magnetic chitosan resin exhibits high performance for the fast removal of uranium from aqueous solutions [9]. In another important paper, Elwakeel reported the remarkable ability of magnetic Schiff's base chitosan composite for the uptake of U(VI) from aqueous media [10].

The dominant species, called uranyl ion, is UO_2^{2+} in cationic form, and it is possible to form complexes with various ions in the hard base behavior with its hard acid feature [11]. Although there are many physicochemical methods for removing low concentration ions or molecules from the aqueous medium, adsorption stands out among these methods with its economic, easy-to-use, and adsorbent design suitable for ions or molecules [12]. Adsorbents such as carbon, natural or synthetic polymers, clays, zeolites, and composite materials are commonly used adsorbents [13]. Composite material, which has gained new properties by combining the properties of different components, has been widely used in adsorption studies in recent years. Saleh published a comprehensive paper about the synthesis of nanomaterials, polymers and green materials as effective adsorbent systems [14]. Some research teams imparted to the literature similar comprehensive paper projects [15–18].

Chitosan, obtained because of deacetylation of chitin, is a biocompatible, biodegradable and non-toxic biopolymer [19]. Chitosan or its composites are used in many researches, depending on their purpose, in areas such as environment, food and medicine [20–22]. At the same time, chitosan is widely used in the removal of various dyes and heavy metals due to the functional groups in its structure. However, chitosan has disadvantages such as easy agglomeration, solubility in acid solutions, and poor strength [23]. These negative properties of chitosan are overcome by forming a composite with various natural minerals [24]. Chitosan composites have resistance to acidic environments, high adsorption capacity for dyes and heavy metals. Vermiculite is an attractive composite material for chitosan due to its low cost, chemical, and mechanical stability.

Vermiculite is one of the widely used clay minerals and has a very high application area in the field of adsorption. It is a 2:1 layered structure (2 octahedral, 1 tetrahedral) alumina silicate minerals [25]. It has been shown to be used in metal adsorption studies due to the presence of exchangeable cations K^+, Ca^{2+}, Mg^{2+} in between the plates [26]. The fact that the metal adsorption capacity is not high has increased the studies to increase the capacity with various surface modifications. Saleh, Tuzen and Sarı synthesized Magnetic vermiculite-modified (MV) by poly (trimesoyl chloride-melamine) (MP) and investigated its efficiency for the removal of bisphenol A. The authors noted that this modified vermiculite is quite effective for the removal of toxic materials like bisphenol A. [27]. In another paper, Salah and coworkers investigated the performance of polyamide-vermiculite nanocomposites for the removal of methylene blue [28].

Lignin is a natural polymer of vegetable origin that occurs as a waste in the paper production process. Considering the amount of waste 50×10^4 metric/ton/year annually, if it can be used, it is economically beneficial [29]. Lignin, which has been shown to be related to metals with various functional groups it carries, can be used as a potential adsorbent, but the solubility of its sulfo form in water limits its use as an adsorbent [30]. For this reason, this problem can be overcome with some modifications or composites that can be formed.

In this study, composites of vermiculite, a natural clay, and two natural polymers lignin and chitosan were made, and the structure of this new material was elucidated using SEM, FT-IR, PZC methods. The adsorbent property of the newly synthesized ternary composite was tested to remove uranyl ions from the aqueous medium. The effects of factors such as concentration, temperature, kinetics and pH on adsorption were investigated. It has been shown that the newly synthesized ternary structure can be used effectively in the adsorption of uranium.

2. Materials and methods

2.1. Chemicals and apparatus

Vermiculite was provided by Akmin Mining (Ankara). Medium molecular weight Ch, 4-(2-pyridylazo) resorcinol (PAR), and $(CH_3COO)_2UO_2{\cdot}2H_2O$ were achieved from Merck (Germany). Sodium tripolyphospate (NaTPP), epichlorohydrin (ECH), lignin, KNO_3, HCl, C_2H_5OH, NaOH, and other chemicals were all purchased from Sigma-Aldrich, Germany. Solutions were prepared in ultrapure water.

2.2. Characterization

The Ch-VL composite adsorbent was characterized by FT-IR (Fourier Transform Infrared Spectroscopy; ATR, Bruker Model: Tensor II), SEM (scanning electron microscopy), and energy-dispersive X-ray spectroscopy (SEM-EDX, TESCAN MIRA3 XMU). The UO_2^{2+} ion concentration was measured with a UV–vis spectrophotometer (SHIMADZU, 160 A model, Japan) at $\lambda = 530$ nm [31].

2.3. Preparation of Ch-VL composite

Approximately 2 g of chitosan, lignin, and vermiculite, each, were mixed in 5% (v/v) acetic acid for 2 h at 250 rpm. The Ch-VL mixture was stirred for 2 h until a homogenous mixture was obtained. Then, 4 mL of epichlorohydrin solution was added to the viscous solution and the final mixture was further stirred for 2 h at 250 rpm, and then left overnight on the bench. On the following day, the Ch-VL mixture was added dropwise into 0.5 M tripolyphosphate solution to mold it into beads. The synthesized Ch-VL composite beads were precipitated and washed five times with distilled water, then the composite was dried at 40 °C and grounded (50 mesh). Finally, a powdered product Ch-VL composite was obtained.

2.4. Batch adsorption experiments

The batch method was used (Table 1). 5000 mg L^{-1} UO_2^{2+} stock solution was prepared. Working solutions were prepared by dilution of the stock AO dye solution with distilled water. The adsorption procedure included 100 mg of Ch-VL composite and 600 mg L^{-1} UO_2^{2+} at natural pH 4.5. Incubation was carried out for 24 h at 25 °C. The absorbance of the final solutions was read at 530 nm. Eqs. (1), (2), and (3). were used to calculate Adsorption%, Q (mol kg^{-1}) and Recovery%.

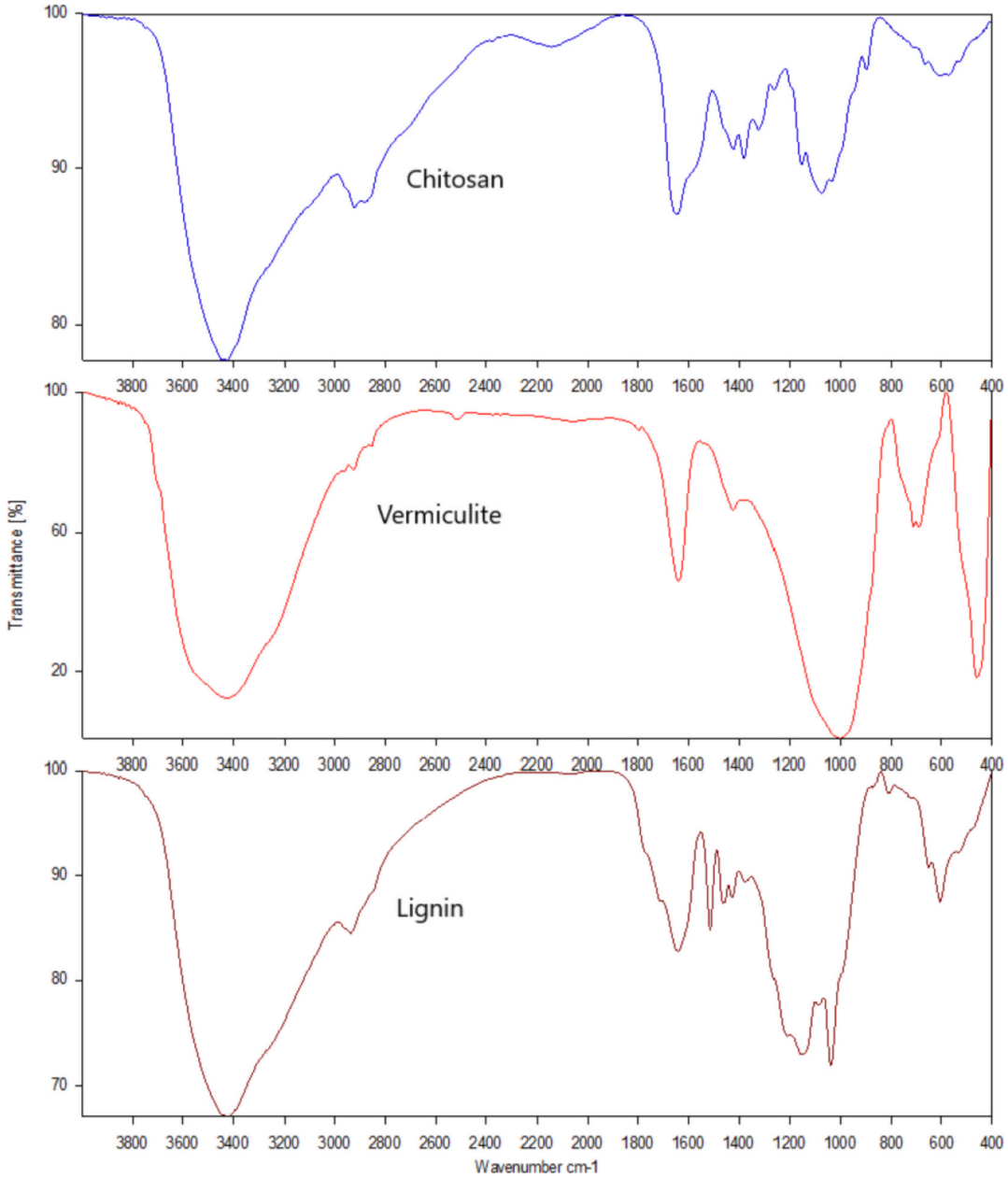

Fig. 1. FT-IR spectra of chitosan, vermiculite and lignin.

$$Adsorption\% = \left[\frac{C_i - C_f}{C_i}\right] \times 100 \quad (1)$$

$$Q = \left[\frac{C_i - C_f}{m}\right] \times V \quad (2)$$

$$Recovery\% = \frac{Q_{des}}{Q_{ads}} \times 100 \quad (3)$$

C_i, the initial concentration of UO_2^{2+} (mg L^{-1}); C_f, the remaining UO_2^{2+} (mg L^{-1}); V, the solution of UO_2^{2+} (L); m, the quantity of the Ch-VL composite (g); Q_{des}, desorbed UO_2^{2+} (mol kg^{-1}); and Q_{ads}, adsorbed UO_2^{2+} (mol kg^{-1}).

2.5. Modeling isotherms

The concentration data obtained to determine the isotherms of the UO_2^{2+} adsorption process were analyzed using Langmuir isotherm (Eq. (4)), Freundlich isotherm (Eq. (5)) and Dubinin-Radushkevich (D-R) isotherm (Eqs. (5)–(8)) models. The Langmuir isotherm model assumes that the active centers where adsorption takes place are homogeneously distributed on the adsorbent surface [32] The Freundlich isotherm model explains a hyperbolic adsorption behavior and gives information about the heterogeneity of the adsorbent surface [33]. The D-R isotherm model assumes that adsorption is related to surface porosity and pore volume. The D-R isotherm model examines adsorption from an energetic point of view and specifies the adsorption process physically or chemically. If the E_{DR} value is in the range of 8–16 kJ mol^{-1}, the adsorption process is chemical, if the E_{DR} is <8 kj mol^{-1}, the adsorption process is physical. The E_{DR} value for this study was within the range of 8–16 kj mol^{-1} [34].

$$Q = \frac{K_L X_L C_e}{1 + K_L C_e} \quad (4)$$

$$Q = X_F C_e^{\beta} \quad (5)$$

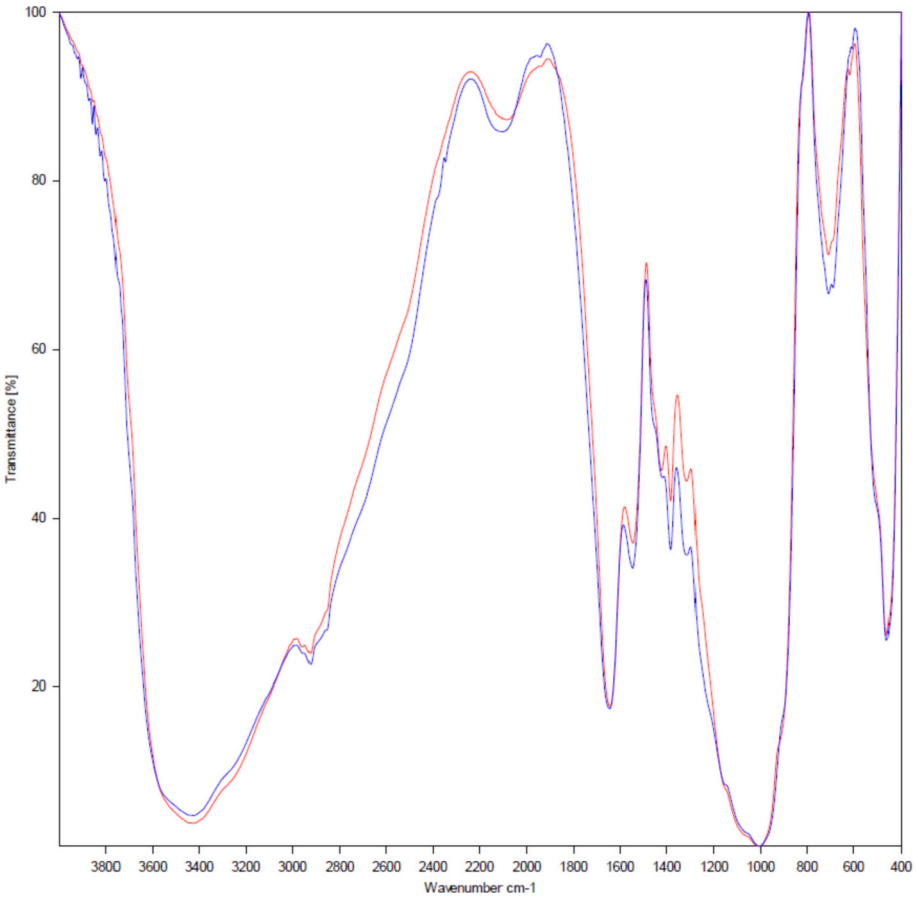

Fig. 2. FT-IR spectra of unloaded Ch-VL (blue) and UO_2^{2+} loaded Ch-VL (red). (For interpretation of the references to colour in this figure legend, the reader is referred to the web version of this article.)

$$Q = X_{DR} e^{-K_{DR}\varepsilon^2} \tag{6}$$

$$\varepsilon = RTln\left(1 + \frac{1}{C_e}\right) \tag{7}$$

$$E_{DR} = (2K_{DR})^{-0.5} \tag{8}$$

X_L: the maximum adsorption capacity (mol kg^{-1}), K_L: the parameter for Langmuir isotherm, Q: the amount of adsorbed UO_2^{2+} (mol kg^{-1}), C_e: the equilibrium concentration (mol L^{-1}), X_F: Freundlich constant, β: adsorbent surface heterogeneity, X_{DR}: a measure of adsorption capacity, K_{DR}: the activity coefficient (mol^2KJ^2), ε: the Polanyi potential, R: the ideal gas constant (8.314 $Jmol^{-1}$ K^{-1}), E_{DR}: the adsorption energy (kj mol^{-1}), T: the absolute temperature (K).

2.6. Modeling kinetics

To explain the mechanism of the adsorption process, the pseudo first order (PFO) (Eq. (9)), pseudo second order (PSO) (Eq. (10)), and intraparticle diffusion (IPD) (Eq. (11)) rate models equations were applied to the experimental data. The PFO model is a model derived based on the adsorption capacity of the adsorbent for a solid-liquid system [35]. The PSO model is based on the solid phase adsorption capacity associated with the number of active centers on the adsorbent surface [36] The IPD model is based on the hypothesis that the adsorption process can be controlled by a combination of one or more factors. These include film diffusion, surface diffusion, pore diffusion, and adsorption on the adsorbent pore surface [37].

$$Q_t = Q_e\left[1 - e^{-k_1 t}\right] \tag{9}$$

$$Q_t = \frac{t}{\left[\frac{1}{k_2 Q_e^2}\right] + \left[\frac{t}{Q_e}\right]} \tag{10}$$

$$Q_t = k_i t^{0.5} \tag{11}$$

Initial rates for the PFO and PSO models of adsorption were calculated using Eqs. (12) and (13), respectively.

$$H_1 = k_1 Q_e \tag{12}$$

$$H_2 = k_2 Q_e^2 \tag{13}$$

Q_t: the adsorbed amount at time (mol kg^{-1}), Q_e: the adsorbed amount at equilibrium (mol kg^{-1}), t: time (min), k_1: the rate constant of the PFO (min^{-1}), H_1: initial adsorption rate for PFO (mol kg^{-1} min^{-1}), k_2: the rate constant of the PSO model (mol^{-1} kg min^{-1}), H_2: initial adsorption rate for PSO (mol kg^{-1} min^{-1}), k_i: the rate constant of the IPD (mol^{-1} kg $min^{-0.5}$).

3. Results and discussion

3.1. FT-IR and SEM-EDX analysis

3.1.1. FT-IR spectra of chitosan (Fig. 1)

Characteristic peaks for chitosan; the absorption bands at 3291–3261 cm^{-1} are the NH and OH stretch, the peaks at 2921 and 2877 cm^{-1} are the CH symmetrical and asymmetric stretching, 1645 cm^{-1} is the C═O stretch of amide I, the 1589 cm^{-1} peak is the NH of the primary amine 1423 and 1375 cm^{-1} peaks are CH_2 bending and CH_3 symmetrical deformations. The 1325 cm^{-1} peak is the C—N stretch of

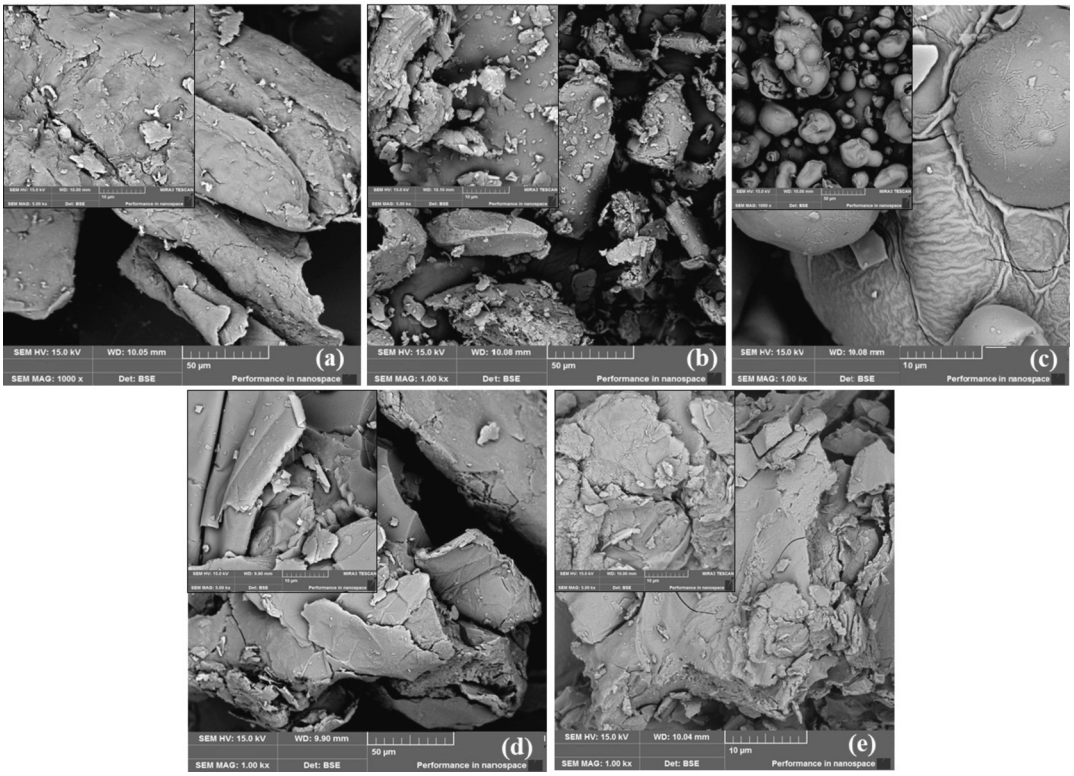

Fig. 3. SEM images of (a) chitosan, (b) vermiculite, (c) lignin, (d) Ch-VL composite, (e) Ch-VL doped with U.

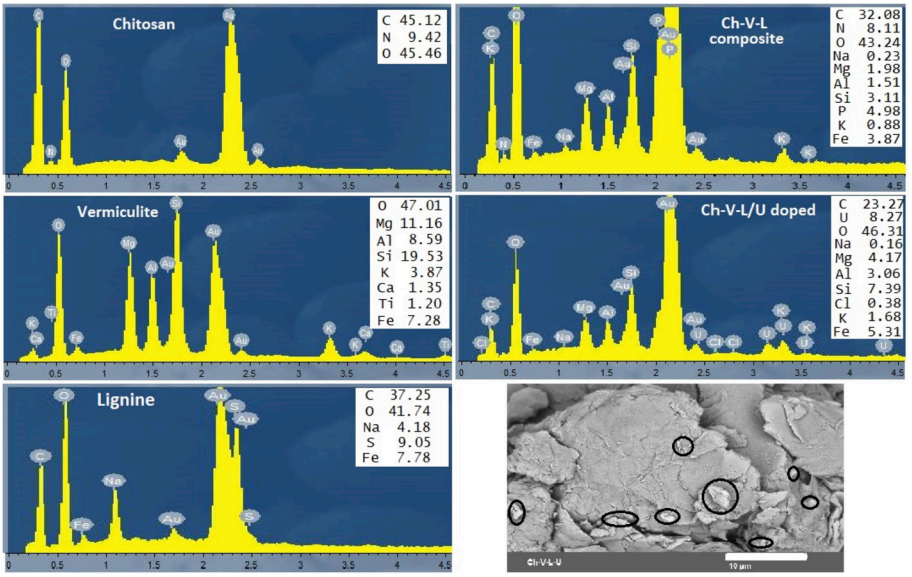

Fig. 4. EDX spectrums of Ch, V, L, Ch-VL and Ch-VL/U doped composites with corresponding quantification results as insets and SEM images of Ch-VL/U doped composite powder.

amide III, the 1550 cm^{-1} peak is the N—H bending of amide II, the 1153 cm^{-1} peak is the asymmetric stretch of the C-O-C bridge. The peaks at 1066–1028 cm^{-1} belong to the C—O stretch [38,39].

3.1.2. FT-IR spectra of vermiculite (Fig. 1)

The peak observed at 3423 cm^{-1} corresponds to the stretching vibrations of OH and silanol groups, while the peak observed at 1631 cm^{-1} corresponds to the bending vibrations of the OH groups, 1012 cm^{-1} corresponds to the stretching vibrations of Si—O and Al—O. while the peak at 466 cm^{-1} corresponds to the vibrations of Si—O—Si, Si—O—Al, Si—O—Al [40].

3.1.3. FT-IR spectra of lignin (Fig. 1)

The peak at 3413 cm^{-1} corresponds to the OH stretching vibration, at 2840 cm^{-1} corresponds to a symmetrical stretching peak for CH_3 of the methoxyl group, while the peak at 2927 cm^{-1} corresponds to the CH stretching in the methyl and methylene group, at 1713 cm^{-1} corresponds to the carbonyl stretch-unconjugated ketone and carboxyl groups, while the peaks at 1508 cm^{-1}, 1458 cm^{-1} and 1426 cm^{-1} correspond to aromatic skeletal vibrations, while the peak at 1119 cm^{-1}

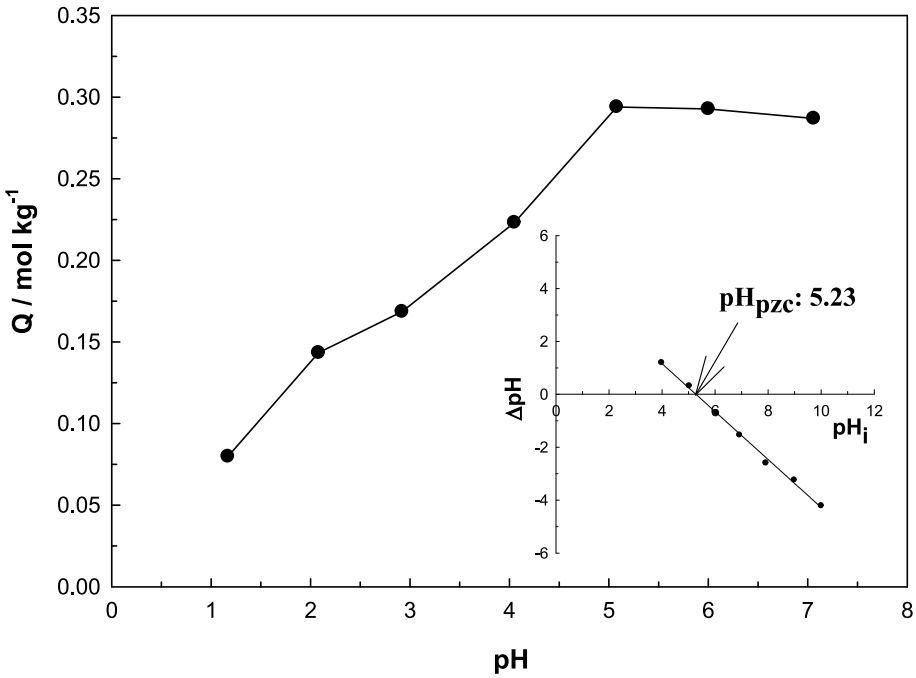

Fig. 5. Effect of pH on adsorption of UO_2^{2+} onto Ch-VL composite. Adsorption conditions: $[UO_2^{2+}]_0$: 600 mg L^{-1}, adsorbent dosage: 100 mg, natural pH:1.0–7.0, contact time:24 h, temperature: 25 °C and PZC for Ch-VL.

corresponds to the ether bond band, corresponds to the peak carbonyl stretch at 1713 cm^{-1}, while the peak at 1035 cm^{-1} corresponds to the CO stretch for the primary alcohol.

3.1.4. FT-IR spectra of the unloaded and loaded Ch-VL (Fig. 2)

It was observed that the peak intensity increased at 1422 cm^{-1} after uranium adsorption was caused by the deformation of the amine groups due to the effect of uranyl ions bound through the amine groups [41]. It is clear that the small amount of deformation at 901–923 cm^{-1} is caused by O═U═O after adsorption due to vermiculite [42,43]. The new peak that appeared at 616 cm^{-1} in the spectrum and the peak that disappeared at 689 cm^{-1} were also evaluated as evidence of uranium adsorption.

Fig. 3 represents the SEM-BSE images of corresponding powders. Chitosan is seen as soft and agglomerated, smooth-surfaced powder with coarse particle size of 250 μm or bigger. Vermiculite is clearly seen as sharp and cleavaged inorganic powders with an average particle size of 35 μm ± 29 μm. Since the standard deviation is huge, the particles are seen as both sharp and dense particles as well as layered structures as indicated in inset pictures. The powders are seen as down to 1 μm and even up to 100 μm as bimodal distribution. Lignin particles are clearly seen as spherical organic powders with an average particle size of 30 μm ± 9 μm that shows a narrower particle distribution than vermiculite with a perfectly spherical shape. Some of the lignin particles are also seen as agglomerated with OH and NH groups to be affected by humidity and coarsened to some extent.

After the composite of Ch-VL was achieved, the layered structure is kept and sharp edges of vermiculite were seen as surrounded by Ch and L due to film-like coating characteristics of organic polymers. The vermiculites are more distributed than a bare condition due to hydrophobic characteristics of organics to keep vermiculite powders separate from each other. Since the vermiculite itself is layer by layer structure as well, the film layers of organics are adapted to its empty spaces and their layers are more uniform and leaf-like that can adsorb any species in-between the layers By the addition of uranyl acetate which reacts to produce uranyl oxide in the oxidative media, the layers are seen to be closed to form more brittle composite structure. The inorganic structure can adsorb U on the surface and also between the layers of both vermiculite and chitosan which formed a composite earlier. The resin structure of lignin holds them all together that has empty bonds which can be said as OH, NH as well as CHs.

Fig. 4 shows the corresponding EDX spectra of mentioned powders and composites and their relative elemental compositions prior to and after U doping. All powders were coated by Au for better conductivity and electron scattering ability but were not included in quantification. Chitosan stands with C-N-O related structure with H species that cannot be counted by SEM-EDX due to low spatial resolution of the smallest element H. Vermiculite is seen as a combination or mixture of silicate-based layered inorganic material which can be counted as illite/cordierite/kaolinite/K feldspathic structures or a mixture of them with small amounts of accompanying iron oxides.

The mixed composite powder is a total combination of three powders on the left column. The mixed powders' quantification has C-N-O from chitosan, C-O-Na and P from lignin and others with O from vermiculite, respectively. The resultant U doped Ch-VL composite has all others in the mixture, indicating a high amount of U adsorption in the composite. The lowest right picture shows the U adsorption on and between the layers of composite as illustrated with black spheres.

3.2. Effect of pH and point of zero charges for Ch-VL

The adsorption process is highly affected by the solution pH, and the solution pH plays an important role in the adsorption process (Fig. 5). In adsorption studies, UO_2^{2+} ions were studied at their natural solution pH. The pH value of 600 mg L^{-1} UO_2^{2+} ion is 4.5. The pH effect on UO_2^{2+} ion adsorption onto Ch-VL composite is shown in Fig. 5. When Fig. 5 is examined, it is seen that dye adsorption increases with increasing pH. It is seen that adsorption increases sharply as the pH increases from 1.0 to 5.0. It was observed that the adsorption decreased slightly in the pH range of 5.0 to 7.0. At pH > 5 values, UO_2^{2+} ions form $UO_2(OH)^+$, $UO_2(OH)_2^{2+}$, $[(UO_2)_3(OH)_5)^+$ forms and precipitate [44]. In this case, precipitation can be perceived as adsorption. It is seen that UO_2^{2+} ion removal is lower at acidic pHs. This is because H^+ ions and cationic UO_2^{2+} ions compete to adsorb onto Ch-VL composite active centers. As a result, UO_2^{2+} ions adsorption to Ch-VL composite is decreased. As the solution pH increases, the electrostatic repulsion forces between the

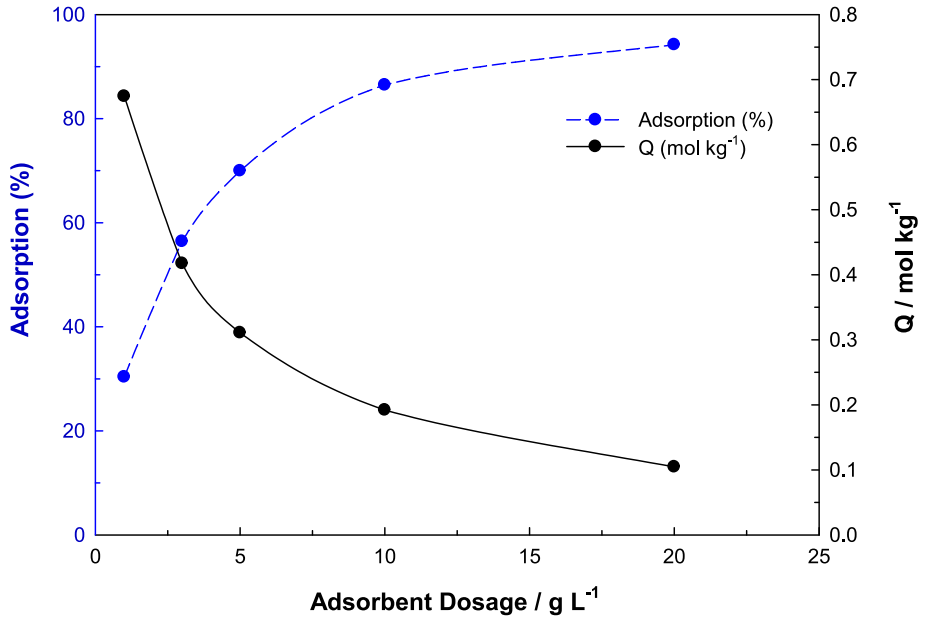

Fig. 6. Effect of adsorbent dosage on adsorption of UO_2^{2+} onto Ch-VL composite. Adsorption conditions: $[UO_2^{2+}]_0$: 600 mg L^{-1}, adsorbent dosage:10, 30,50, 100 and 200 mg, natural pH:4.5, contact time:24 h, temperature: 25 °C.

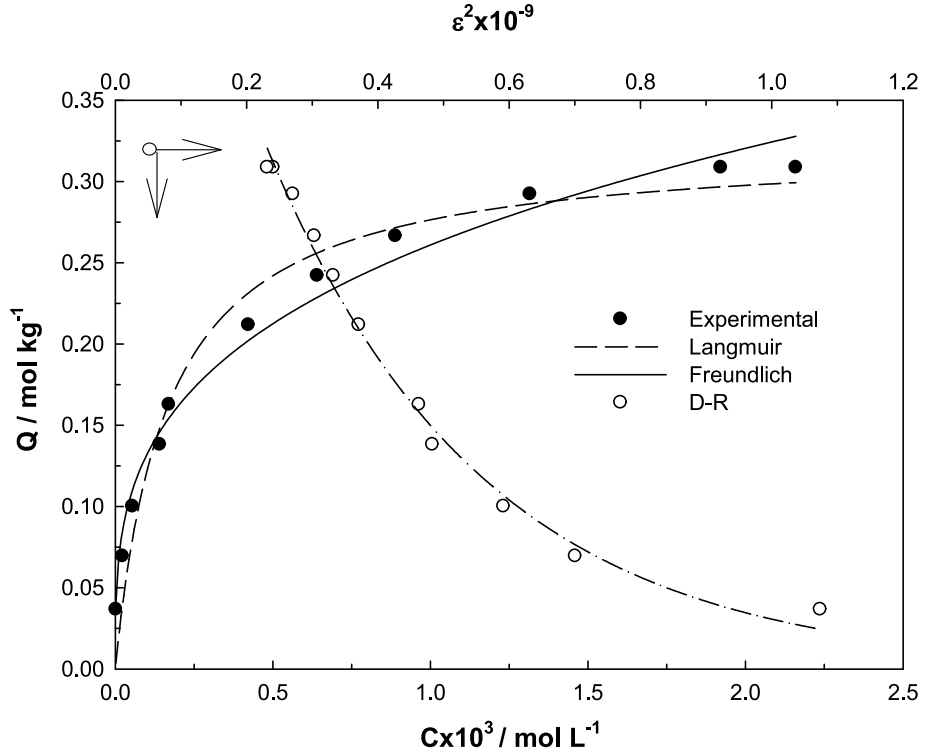

Fig. 7. Experimentally obtained adsorption isotherms UO_2^{2+} onto Ch-VL composite and their compatibility to Langmuir, Freundlich, and D-R models. Adsorption conditions: $[UO_2^{2+}]_0$: 50–1000 mg L^{-1}, adsorbent dosage:100 mg, natural pH:4.5, contact time:24 h, temperature: 25 °C.

UO_2^{2+} ions and the Ch-VL composite surface decrease, resulting in an increase in UO_2^{2+} ions adsorption. At basic pHs, the surface of the Ch-VL composite is negatively charged and H-bonds and van der Waals interactions can be seen between the UO_2^{2+} ions and the Ch-VL composite, so adsorption is seen to be high.

The solution pH value at which the surface charge of the adsorbent is zero is defined as the point of zero charge (pzc). In order to determine the PZC value of the Ch-VL composite, the Ch-VL composite was kept in solutions containing 0.1 mol L^{-1} KNO_3 in the pH = 1.0–12.0 range for 24 h and the equilibrium pH was measured. 0.1 M HCl or NaOH was used to adjust the pH. The PZC value was obtained from the linear relationship between the initial pHi and ΔpH. The ΔpH value was obtained from the difference between the initial and final pH ($\Delta pH = pH_f - pH_i$). The surface charge of the Ch-VL composite was found to be 5.23 (Fig. 5). The surface of the Ch-VL composite was positive (pH < pHpzc) below pH 5.23 and negative (pH > pHpzc) above pH 5.23. The condition pH > pHpzc explains the increasing.

Table 2
Langmuir, Freundlich and D-R isotherm models and their parameters.

Isotherm models	Parameter	Value	R^2
Langmuir	X_L (mol kg^{-1})	0.322	0.965
	K_L (L mol^{-1})	6023	
Freundlich	X_F	2.02	0.985
	β	0.296	
D-R	X_{DR} (mol kg^{-1})	0.651	0.993
	$-K_{DR}x10^9$/mol^2KJ^{-2}	3.05	
	E_{DR}/kJ mol^{-1}	12.8	

3.3. Effect of adsorbent dosage

Adsorbent dosage is an important parameter that affects the adsorption process by affecting the adsorption capacity of the adsorbent. The effect of the amount of Ch-VL composite on UO_2^{2+} ion adsorption onto Ch-VL composite is presented in Fig. 6. When Fig. 6 is examined, a sharp increase in dye adsorption is observed. This initial increase is due to the high number of active centers on the Ch-VL composite surface. Afterward, it was observed that the adsorption remained almost constant. This is due to the fact that all UO_2^{2+} ions are attached to the Ch-VL composite surface and the balance between the UO_2^{2+} ions on the adsorbent surface and the UO_2^{2+} ions in the solution has been established. It was thought that the adsorption may have increased with the increase in the amount of adsorbent, with the effect of the functional groups such as amine, hydroxyl in the surface of the Ch-VL composite.

3.4. Adsorption isotherm models

Adsorption isotherms were used to demonstrate the interaction mechanism between adsorbent and UO_2^{2+} ions at equilibrium. Comparing the R^2 values derived from the Langmuir and Freundlich isotherm models (Fig. 7, Table 2), it can be seen that the adsorption process conformed to the Freundlich isotherm model. UO_2^{2+} ion adsorption on Ch-VL provided a better fit with the Freundlich model (R^2 = 0.985). X_F, which is a measure of adsorption capacity, was 2.02, and β surface heterogeneity was 0.296, from the Freundlich isotherm model. The β surface heterogeneity showed that the conditions were favorable for the adsorption. The maximum adsorption capacity was 0.322 mol kg^{-1} and the K_L value was 6023 L mol^{-1}. The high adsorption capacity of Ch-VL composite is promising for its use as an adsorbent for the removal of UO_2^{2+} ions from water or wastewater. X_F, which is a measure of adsorption capacity, was 2.02, and β surface heterogeneity was 0.296, from Freundlich isotherm model. The magnitude of the E_{DR} value in the D-R model characterizes the type of adsorption process (Fig. 7). (Table 2). The adsorption energy, 12.8 kJ mol^{-1}, derived by the D-R model, suggested that the nature of the adsorption is chemical.

3.5. Adsorption kinetics

To analyze the adsorption kinetics, PFO, PSO and IPD rate models equations were applied to the experimental data. It could be said that UO_2^{2+} ion adsorption occurred at two stages (Fig. 8). In the first stage, rapid adsorption took place, involving the first 360 min (6 h). In the second phase, there was longer and slower adsorption, possibly involving the interior of the adsorbent. The first stage was fast and quantitatively dominant, and the second stage was slower and quantitatively insignificant. During the initial stage of adsorption, there were many available active centers on the Ch-VL surface. After these centers were occupied, the equilibrium state was realized, and the second stage was started, involving the inner regions of the adsorbent.

The rapid stage results from the abundance of active centers on the

Table 3
PFO, PSO and IPD kinetic models and their parameters.

Kinetic models	Parameter	Value	R^2
PFO	Q_t/mol kg^{-1}	0.221	
	Q_e/mol kg^{-1}	0.253	0.972
	$k_1 \times 10^3$/mol^{-1} kg min^{-1}	10.1	
	$H \times 10^3$/mol kg^{-1} min^{-1}	2.21	
PSO	Q_t/mol kg^{-1}	0.221	0.981
	Q_e/mol kg^{-1}	0.218	
	$k_2 \times 10^3$/mol^{-1}kg min^{-1}	49.8	
	$H \times 10^3$/mol kg^{-1} min^{-1}	3.18	
IPD	$k_i \times 10^3$/mol kg^{-1} $min^{-0.5}$	1.54	0.989

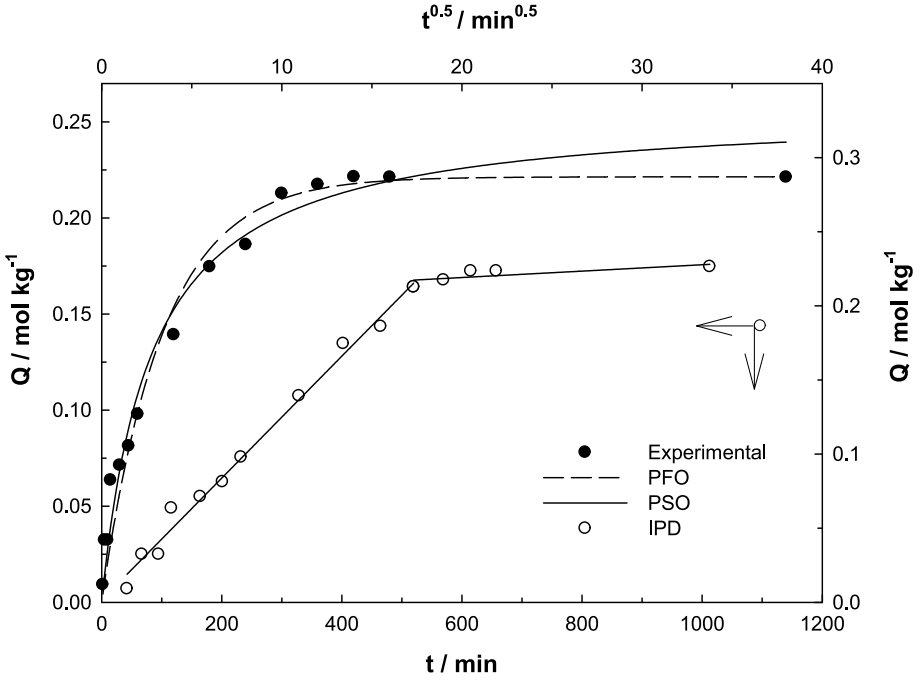

Fig. 8. Compatibility of UO_2^{2+} adsorption kinetics to PFO, PSO and IPD models. Adsorption conditions: $[UO_2^{2+}]_0$: 600 mg L^{-1}, adsorbent dosage: 300 mg, natural pH: 4.5, contact time: 2–1440 min, temperature: 25 °C.

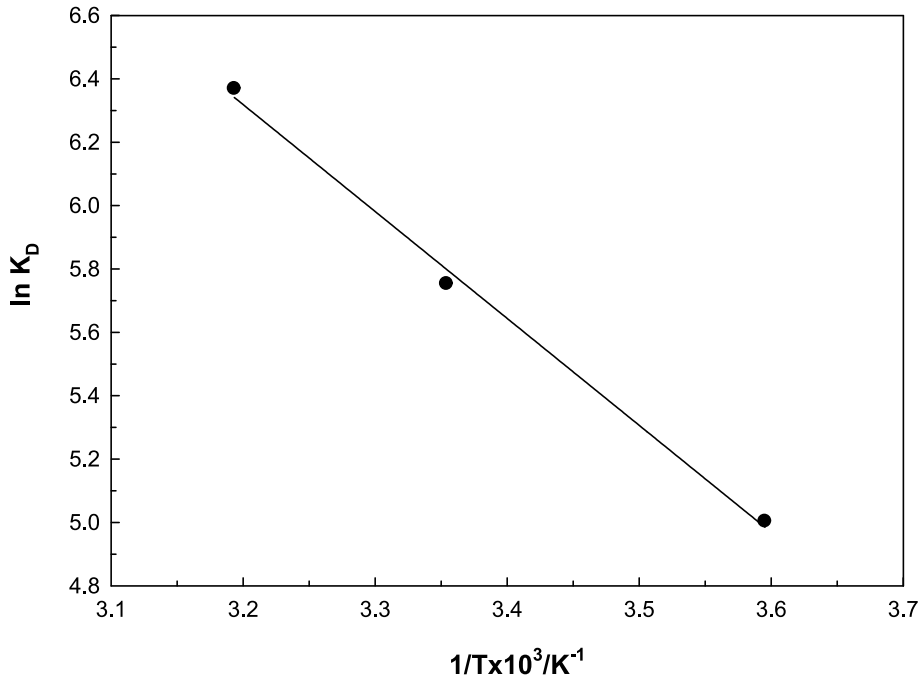

Fig. 9. The effect of temperature on the adsorption. Adsorption conditions: $[UO_2^{2+}]_0$: 600 mg L^{-1}, adsorbent dosage: 100 mg, natural pH: 4.5, contact time: 24 h, temperature: 5 °C, 25 °C and 40 °C.

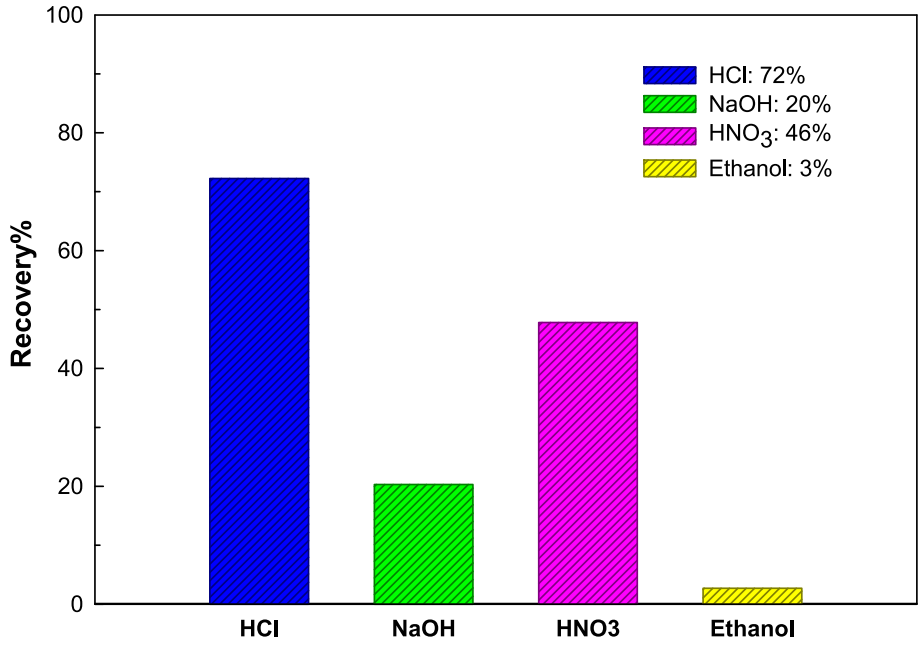

Fig. 10. The effect of recovery for Ch-VL. Adsorption conditions: $[UO_2^{2+}]_0$: 600 mg L^{-1}, adsorbent dosage:100 mg, natural pH:4.5, contact time:24 h, temperature: 25 °C.

Ch-VL composite surface, while the gradual filling of these sites also makes the adsorption process less efficient during the slower stage. In the first stage of adsorption, there are many active centers on the Ch-VL composite surface. UO_2^{2+} ions are adsorbed to these active centers. Over time, the number of active centers on the Ch-VL composite surface decreases, and the UO_2^{2+} ions become saturated. In the next step, the UO_2^{2+} ions diffuse slowly through the pore of the Ch-VL composite. Therefore, adsorption slows down.

When the correlation coefficients (R^2) of the PFO and PSO models were compared with each other, it was seen that the results fit the PSO kinetic model better. In addition, the closeness of the theoretically calculated Q_t and experimental Q_e values showed compatibility with the PSO model. These results showed that the adsorption process followed the PSO rate kinetics. Furthermore, the multi-linear curves seen in the IPD plot indicated that the adsorption process involved two or more steps, as highlighted above. In this case, it was shown that it is not possible to explain the adsorption with a single kinetic model. UO_2^{2+} ions first rapidly filled the active centers on the surface of the Ch-VL composite and then diffused slowly and gradually through the pore of the Ch-VL composite. The adsorption process is accompanied by surface

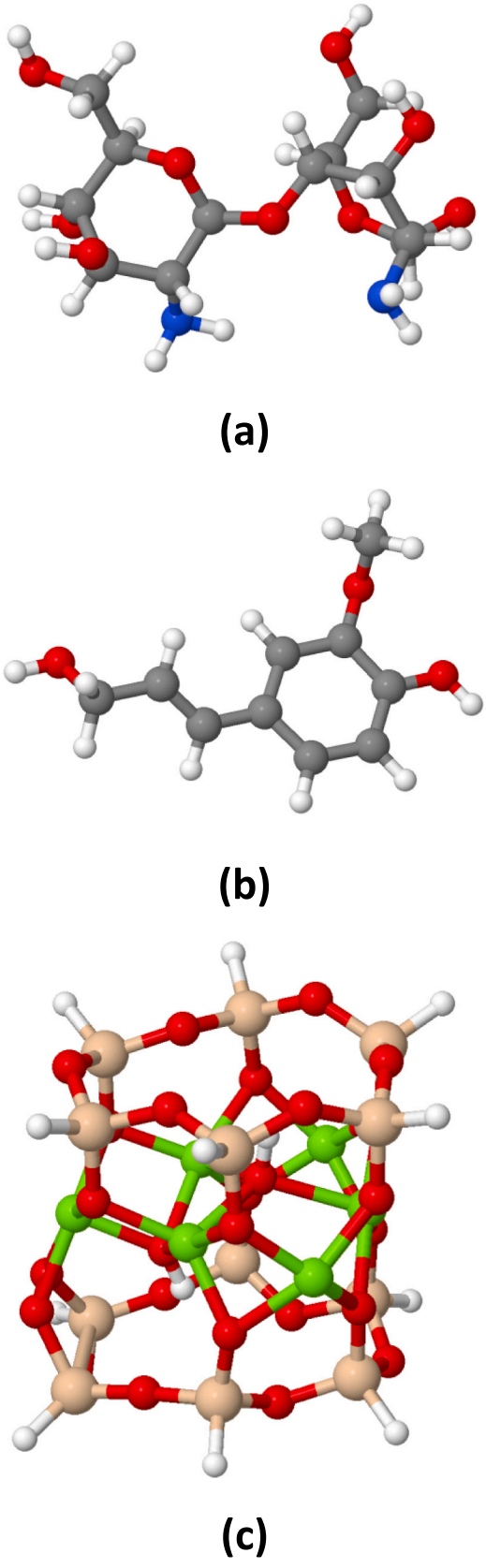

Fig. 11. Finite-size atomistic models of chitosan (a), lignin (b) and vermiculite (c).

diffusion, film diffusion, diffusion on the pore surface or more than one of these steps (see Table 3).

3.6. Adsorption thermodynamics

To interpret the thermodynamic behavior of the adsorption process, temperatures of 5 °C, 25 °C, and 40 °C were studied (Fig. 9). The change in ΔH^0 during the adsorption process was 28.1 kJ mol^{-1}. In the endothermic adsorption process, temperature rise had a positive effect on UO_2^{2+} ion removal; The amount adsorbed increased with increasing temperature. The entropy change, ΔS^0, was 142 $Jmol^{-1}$ K^{-1}. This finding indicated the randomness of the adsorption process. A positive entropy could be interpreted as an increase in the randomness of the adsorption system due to the high affinity of the adsorbent [45]. ΔG^0s were −11.4 kJ mol^{-1}, −14.4 kJ mol^{-1} and −16.4 kJ mol^{-1} at 5 °C, 25 °C, and 40 °C, respectively. The greater availability of ΔG^0 at higher temperatures was due to increased mobility of UO_2^{2+} ions on the Ch-VL composite surface, increased electrostatic interaction between UO_2^{2+} ions and different functional groups on the Ch-VL composite surface and chemical potential changes related to the solubility of UO_2^{2+} ions thought to be possible.

3.7. Adsorption mechanism

The mechanism of attachment of UO_2^{2+} ions onto Ch-VL composite can be explained by the strong attraction forces of functional groups on the composite surface. The functional groups on the surface of Ch-VL composite were mainly such as amine, hydroxyl groups (confirmed by the FT-IR spectrum) [46]. It could be very likely that electrostatic attraction plays an important role in the adsorption of UO_2^{2+} ions. For a general mechanism, following explanation was suggested: (i) migration of the UO_2^{2+} ions onto the surface of the Ch-VL composite (bulk solution transport), (ii) diffusion of the UO_2^{2+} ions across the boundary layer to the surface of the Ch-VL composite (film diffusion), (iii) adsorption of the UO_2^{2+} ions onto the surface of the Ch-VL composite. –OH, NH_2 groups and O bridges on the surface of Ch-VL composite form adsorption sites. The –OH and NH_2 groups of the Ch-VL composite could form H-bonds with the UO_2^{2+} ions and function as adsorption centers.

The final stage of the adsorption process could involve the penetration of some UO_2^{2+} ions into the Ch-VL composite via intra particle diffusion. In the light of this information, it is thought that the adsorption process of UO_2^{2+} ions in The Ch-VL composite is accompanied by surface diffusion, film diffusion, intra particle diffusion and diffusion on the pore surface.

3.8. Recovery

Three consequential adsorption and desorption cycles were executed using HCl, NaOH for desorption (Fig. 10). It was shown that the highest recovery of the adsorption activity was with HCl, 72%. This indicated that after the three recycling process Ch-VL composite retained 72% of its initial adsorption capacity. And these findings were taken as the proof that Ch-VL composite could be an alternative adsorbent in the recycling of UO_2^{2+} ions from industrial aqueous wastewaters.

4. Theoretical study

4.1. Structure of the adsorbent

Vermiculite is a periodic crystal, whereas chitosan and lignin are polymers. To represent the adsorbent, we used simple finite-size H-terminated atomistic models $C_{12}N_2H_{24}O_9$, $C_{10}H_{12}O_3$ and $Mg_6Si_{12}H_{14}O_{26}$ for chitosan, lignin and vermiculite, respectively (see Fig. 11). Then we tried different geometries of $C_{12}N_2H_{24}O_9$ + $C_{10}H_{12}O_3$ complex and chose the lowest energy structure (Fig. 12). As expected, $C_{12}N_2H_{24}O_9$ and $C_{10}H_{12}O_3$ formed a hydrogen bond. Similarly, we constructed a

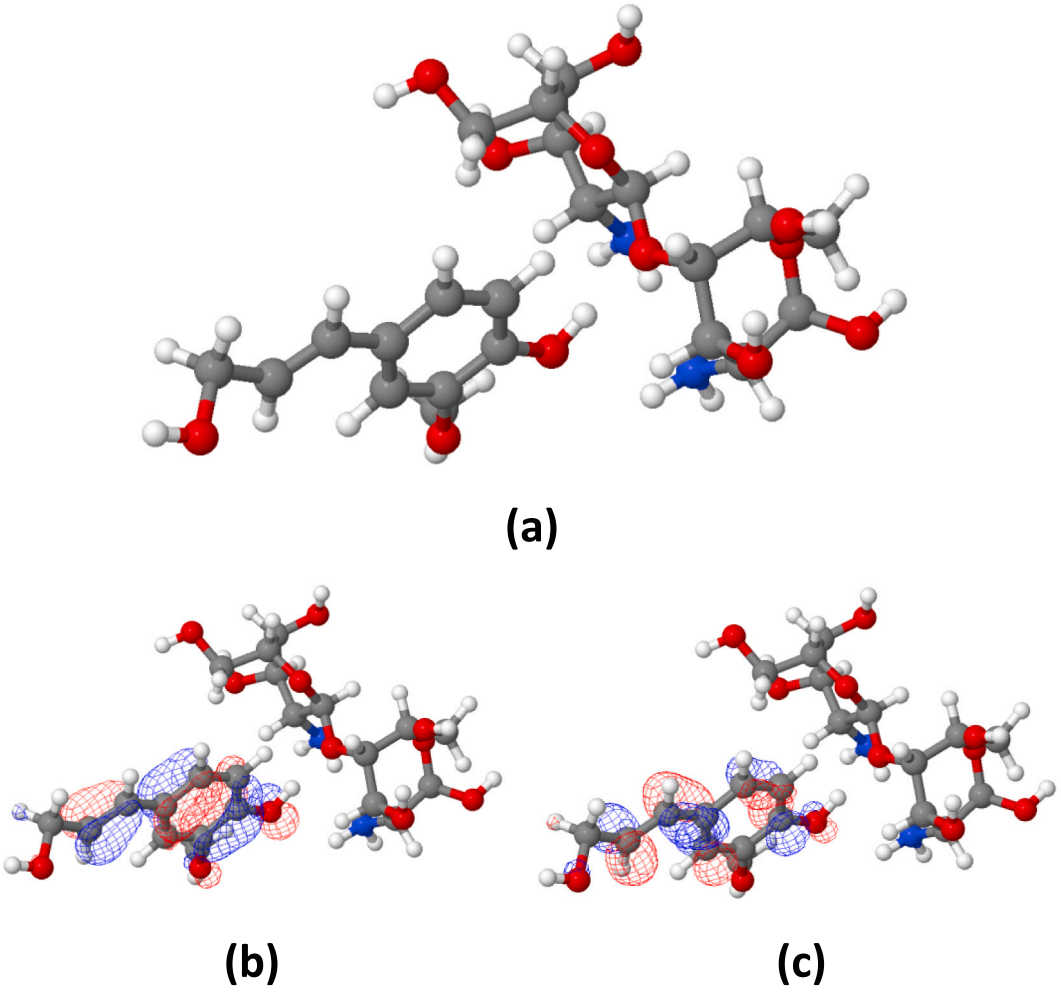

Fig. 12. Structure (a), and frontier orbitals HOMO (b) and LUMO (c) of the $C_{12}N_2H_{24}O_9$ + $C_{10}H_{12}O_3$ complex.

complex "$C_{12}N_2H_{24}O_9 + C_{10}H_{12}O_3 + Mg_6Si_{12}H_{14}O_{26}$", consisted of three components linked by hydrogen bonds (Fig. 13).

All calculations were performed with the B3LYB functional [47,48] and 6-31G*_ldz electronic basis set for magnesium combined with the 6-31G** set for others elements [49]. Van-der-Waals interaction was introduced through the Grimme's D3 dispersion corrections [50]. GeoMeTRIC algorithm was applied for rapid geometry optimizing [51] as it is implemented in GPU-oriented TeraChem software [52]. JMol software was used for visualization [53].

In the Conceptual Density Functional Theory (CDFT), chemical hardness is defined as the second derivative with respect to number of electrons (N) of total electronic energy (E) at a constant external potential, υ(r) (see Table 4).

$$\eta = \left[\frac{\partial^2 E}{\partial N^2}\right]_{\nu(r)} \tag{14}$$

In the light of the finite differences approach, to calculate the chemical hardness of any system, the following equation based on ground state ionization energy (I) and ground state electron affinity (A) is derived.

$$\eta = I - A \tag{15}$$

Ground state ionization energy and ground state electron affinity of the chemical systems can be approximately predicted using Koopmans Theorem. This theorem presents the relations with frontier orbital energies of ground state ionization energy (I) and ground state electron affinity as:

$$I = -E_{HOMO} \quad \text{and} \quad A = -E_{LUMO} \tag{16}$$

In Table 1, Calculated properties of $C_{12}N_2H_{24}O_9$ (chitosan), $C_{10}H_{12}O_3$ (lignin) and $Mg_6Si_{12}H_{14}O_{26}$ (vermiculite) molecules and their complexes are presented. Chemical hardness is reported as the resistance against electron cloud polarization of chemical systems. Hard and Soft Acid-Base Principle states that hard acids prefer to coordinate to hard bases and soft acids prefer to coordinate to soft bases. Hard chemical systems are not polarizable while soft chemial systems exhibit high polarization. Minimum Polarizability Principle states that in a stable state, polarizability is minimized [54]. Some researchers noted that dipole moment can be used as a measure of the polarizability of the compounds. Koopmans Theorem can be considered as a bridge between Conceptual DFT and Molecular Orbital Theory. Molecular Orbital Theory uses frontier orbital energies to predict the acidic or basic behaviors of molecules. The molecules with higher value of HOMO orbital energy are good electron donors. According to Maximum Hardness Principle (MHP) proposed by Pearson, chemical hardness is a useful indicator of the stability. Through MHP, it can be noted that hard chemical systems are more stable compared to others. Calculated binding energies for the studied chemical systems show that the components of the composite material strongly interact with each other. In the light of calculated HOMO energy, chemical hardness and dipole moment values, it can be said that the most stable chemical system among the studied matters is chitosan. Density Functional Theory considers the electron density to describe the chemical reactivity of the chemical systems. Thanks to DFT calculations, reactive centers, reactivity and stabilities of the chemical

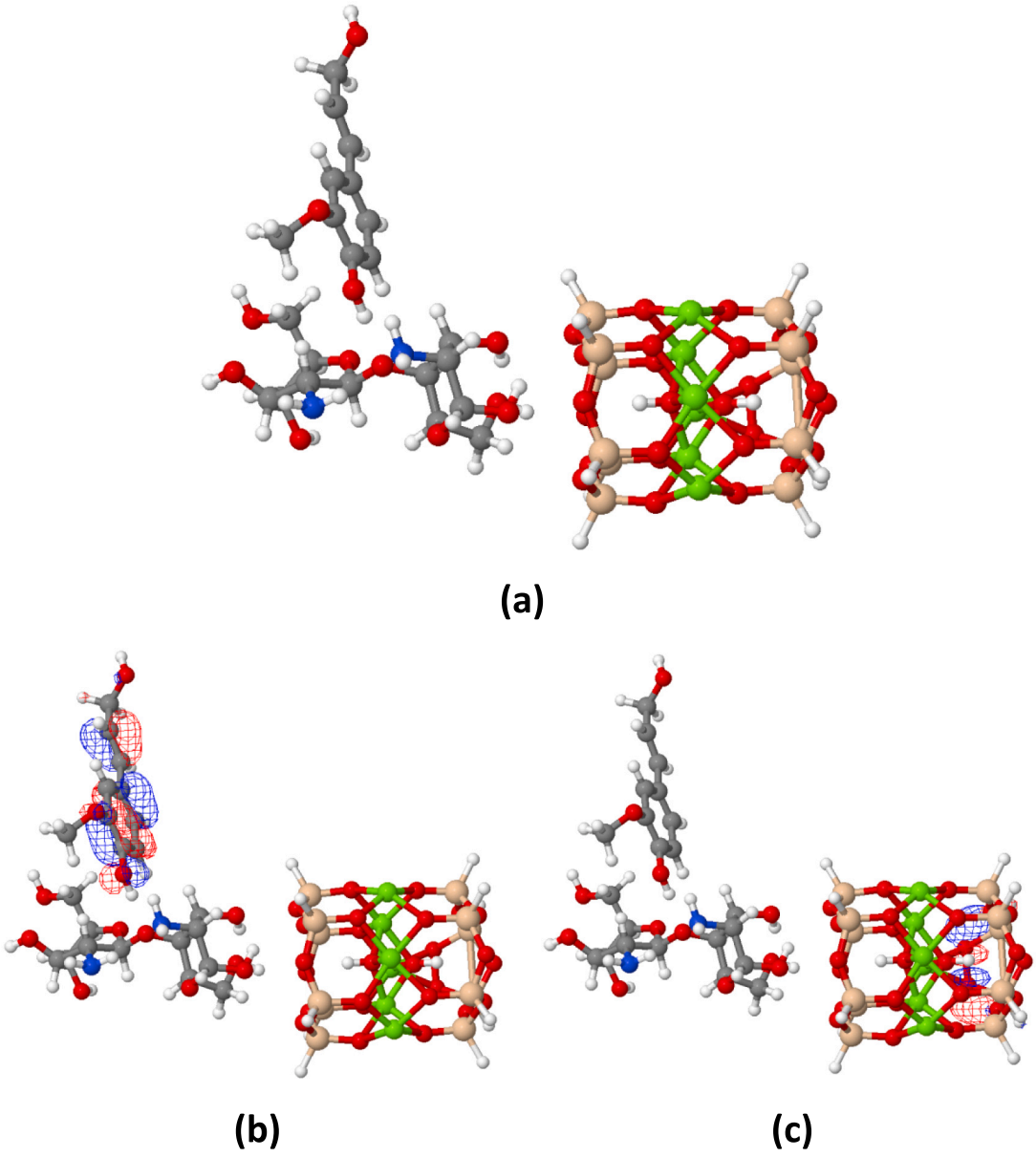

Fig. 13. Structure (a), and frontier orbitals HOMO (b) and LUMO (c) of the $C_{12}N_2H_{24}O_9$ + $C_{10}H_{12}O_3$ + $Mg_6Si_{12}H_{14}O_{26}$ complex.

Table 4
Calculated properties of $C_{12}N_2H_{24}O_9$ (chitosan), $C_{10}H_{12}O_3$ (lignin) and $Mg_6Si_{12}H_{14}O_{26}$ (vermiculite) molecules and their complexes. Binding energies of complexes E_b are calculated as the energy differences between two or three components and corresponding complex.

	E_b, eV	HOMO, eV	LUMO, eV	η, eV	D, Debye
$C_{12}N_2H_{24}O_9$	–	−5.99	1.50	7.49	2.96
$C_{10}H_{12}O_3$	–	−5.38	−0.54	4.84	3.24
$Mg_6Si_{12}H_{14}O_{26}$	–	−7.79	−3.06	4.72	8.59
$C_{12}N_2H_{24}O_9$ + $C_{10}H_{12}O_3$	0.71	−5.13	−0.37	4.76	4.78
$C_{12}N_2H_{24}O_9$ + $C_{10}H_{12}O_3$ + $Mg_6Si_{12}H_{14}O_{26}$	1.73	−5.03	−3.16	1.87	10.86

systems can be easily predicted. In the literature, some similar studies were published. For example, V.K. Gupta and coworkers investigated spectroscopic and computational evaluation of cadmium adsorption on activated carbon [55].

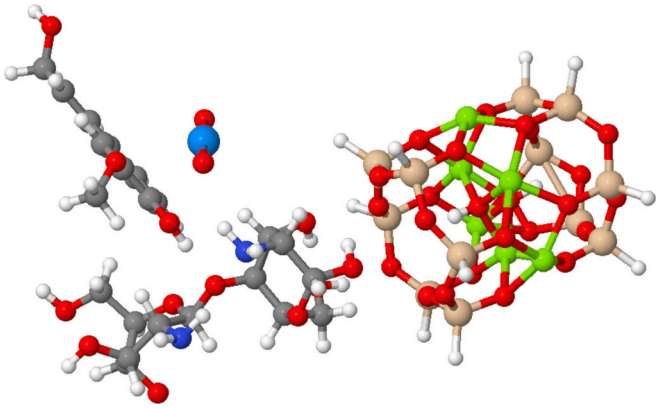

Fig. 14. Adsorption of uranyl UO_2^{2+} on complex adsorbent presented in Fig. 13.

Table 5
Comparison of sorption capacities of other chitosan-based sorbents for UO_2^{2+} removal.

Adsorbent type	pH	Temperature (°C)	Q_{max} (mol kg^{-1})	References
Epichlorohydrin cross-linked chitosan	3.0	25	0.268	[57]
Graphene oxide–chitosan	–	–	0.187	[58]
Amidoxime modified chitosan/bentonite			0.181	[59]
Chitosan@attapulgite	5.5	25	0.0420	[60]
Chitosan modified phosphate rock	2.5	25	0.0364	[61]
Diethylenetriamine-modified magnetic chitosan resins	3.5	25	0.293	[62]
Chitosan-sepiolite	4.5	25	0.220	[31]
Ch-VL composite	4.5	25	0.322	This study

4.2. Interaction of the adsorbent with uranyl UO_2^{2+}

As a next step, we considered the adsorption of uranyl onto the resulting adsorbent. Note that the B3LYP functional used describes adsorption well and provides agreement with the experiments for the case of both hydrogen and organometallic binding. Uranium is the heavy element with *f*-orbitals, which are unavailable in TeraChem. Therefore, we used another software, Quantum Espresso, to investigate adsorbent binding with uranyl UO_2^{2+}. We used the same method, as was earlier described in Ref. [56] for vermiculite-uranyl interaction. Fig. 14 presents the preferred adsorption site for uranyl (see Fig. 14). The adsorption energy calculated as E (adsorbent) + E (UO_2^{2+}) − E (adsorbent + UO_2^{2+}) is 0.47 eV. This calculated value implies that the new composite material acts as a powerful adsorbent for the effective removal of uranyl ions.

5. Comparison of adsorbents studied in the literature

UO_2^{2+} ions adsorption capacities of various adsorbents were compared (Table 5) and the adsorption capacity of the admass of Ch-VL composite was found to be the second highest (0.322 mol kg^{-1}). This adsorption advantage might have been derived from the richness of the functional groups on the Ch-VL composite surface. In addition, Ch-VL composite is an easily obtained adsorbent. Therefore, the use of Ch-VL composite as an adsorbent is an economical initiative that is needed for wastewater treatment processes due to its low cost, environmentally friendly, easy and economical preparation and inexpensive adsorbent.

6. Conclusion

The results of this study showed that newly synthesized ternary structure (Ch-VL) was highly efficient in the removal- and recovery of UO_2^{2+} ions in aqueous solution. The adsorption process was investigated in terms of initial pH, initial UO_2^{2+} ions concentration, temperature, amount of composite, contact time, temperature and recovery. Various adsorption isotherms were applied to the experimental findings. The results obtained from the Langmuir isotherm model showed that the UO_2^{2+} ions onto Ch-VL composite have a maximum adsorption capacity of 0.322 mol kg^{-1}. Adsorption kinetics showed that the process of UO_2^{2+} ions adsorption was suited to the PSO and IPD models. UO_2^{2+} ions first rapidly filled the active centers on the surface of the Ch-VL composite, and then slowly and gradually diffused through the pore of the Ch-VL composite. Thermodynamic findings, $\Delta H > 0$, $\Delta S > 0$, and $\Delta G < 0$, showed that adsorption behavior was endothermic and spontaneous. Recovery studies have revealed that Ch-VL composite was recyclable at least three times. UO_2^{2+} ions adsorption onto Ch-VL composite was supported by FT-IR and SEM-EDX analyses. To sum up, the findings of this research provided a simple and cost-effective approach for the removal of toxic UO_2^{2+} ions from wastewaters. The nature of the chemical interactions between studied chemical systems was analyzed in the light of Density Functional Theory calculations. DFT calculations provided compatible results with the experiments made. Both calculations and experiments showed that the new composite material is a powerful adsorbent for the effective removal of uranyl ions. The nature of the chemical interactions between studied chemical systems was analyzed in the light of density functional theory calculations, which provided compatible results with the experiments made. Both calculations and experiments showed that new composite material is a powerful adsorbent for the effective removal of uranyl ions.

CRediT authorship contribution statement

Zeynep Mine Şenol: Writing - Original Draft, Investigation, Writing - Review & Editing.

Savaş Kaya: Writing - Original Draft, Investigation, Writing - Review & Editing, Software.

Selçuk Şimşek: Conceptualization, Methodology, Supervision, Writing - Original Draft, Writing - Review & Editing.

K.P. Katin: Methodology, Writing - Original Draft, Software.

Ali Özer: Formal analysis, Methodology, Writing.

Riadh Marzouki: Software, Writing, Funding acquisition.

Acknowledgments

The authors extend their appreciation to the Deanship of Scientific Research at King Khalid University for funding this work through a research groups program under grant number R.G.P.2/71/42. The present study was partly supported by Sivas Cumhuriyet University Scientific Research Projects Commission. The authors have declared no conflict of interest.

References

[1] Y. Dai, L. Zhou, X. Tang, J. Xi, J. Ouyang, Z. Liu, A.A. Adesina, Macroporous ion-imprinted chitosan foams for the selective biosorption of U (VI) from aqueous solution, Int. J. Biol. Macromol. 164 (2020) 4155–4164.
[2] R. Rostamian, M. Firouzzare, M. Irandoust, Preparation and neutralization of forcespun chitosan nanofibers from shrimp shell waste and study on its uranium adsorption in aqueous media, React. Funct. Polym. 143 (2019), 104335.
[3] W. Liu, L. Zhang, F. Chen, H. Wang, Q. Wang, K. Liang, Efficiency and mechanism of adsorption of low-concentration uranium from water by a new chitosan/aluminum sludge composite aerogel, Dalton Trans. 49 (10) (2020) 3209–3221.
[4] S. Xie, J. Yang, C. Chen, X. Zhang, Q. Wang, C. Zhang, Study on biosorption kinetics and thermodynamics of uranium by Citrobacter freudii, J. Environ. Radioact. 99 (1) (2008) 126–133.
[5] A.P. Gilman, D.C. Villeuve, V.E. Secours, A.P. Yagminas, B.L. Tracy, J.M. Quinn, M. A. Moss, Uranyl nitrate: 28-day and 91-day toxicity studies in the Sprague-Dawley rat, Toxicol. Sci. 41 (1) (1998) 117–128.
[6] M.F. Hamza, Y. Wei, M.S. Khalafalla, N.S. Abed, A. Fouda, K.Z. Elwakeel, N. A. Hamad, U (VI) and Th (IV) recovery using silica beads functionalized with urea- or thiourea-based polymers–application to ore leachate, Sci. Total Environ. 153184 (2022).
[7] M.F. Hamza, A. Fouda, K.Z. Elwakeel, Y. Wei, E. Guibal, N.A. Hamad, Phosphorylation of guar gum/magnetite/chitosan nanocomposites for uranium (VI) sorption and antibacterial applications, Molecules 26 (7) (2021) 1920.
[8] K.Z. Elwakeel, M.F. Hamza, E. Guibal, Effect of agitation mode (mechanical, ultrasound and microwave) on uranium sorption using amine-and dithizone-functionalized magnetic chitosan hybrid materials, Chem. Eng. J. 411 (2021), 128553.
[9] K.Z. Elwakeel, A.A. Atia, E. Guibal, Fast removal of uranium from aqueous solutions using tetraethylenepentamine modified magnetic chitosan resin, Bioresour. Technol. 160 (2014) 107–114.
[10] K.Z. Elwakeel, A.A. Atia, Uptake of U (VI) from aqueous media by magnetic Schiff's base chitosan composite, J. Clean. Prod. 70 (2014) 292–302.
[11] N.H. Elsayed, R.A. Alatawi, M. Monier, Amidoxime modified chitosan based ion-imprinted polymer for selective removal of uranyl ions, Carbohydr. Polym. 256 (2021), 117509.
[12] Y. Dai, L. Zhou, X. Tang, J. Xi, J. Ouyang, Z. Liu, A.A. Adesina, Macroporous ion-imprinted chitosan foams for the selective biosorption of U (VI) from aqueous solution, Int. J. Biol. Macromol. 164 (2020) 4155–4164.
[13] S. Şimşek, Adsorption properties of lignin containing bentonite-polyacrylamide composite for UO22+ ions, Desalin. Water Treat. 57 (50) (2016) 23790–23799.

[14] T.A. Saleh, Protocols for synthesis of nanomaterials, polymers, and green materials as adsorbents for water treatment technologies, Environ. Technol. Innov. 24 (2021), 101821.
[15] J. Wang, Z. Shi, J. Fan, Y. Ge, J. Yin, G. Hu, Self-assembly of graphene into three-dimensional structures promoted by natural phenolic acids, J. Mater. Chem. 22 (42) (2012) 22459–22466.
[16] T.A. Saleh, Experimental and analytical methods for testing inhibitors and fluids in water-based drilling environments, TrAC Trends Anal. Chem. 116543 (2022).
[17] T.A. Saleh, Advanced trends of shale inhibitors for enhanced properties of water-based drilling fluid, Upstream Oil and Gas Technology 8 (2022), 100069.
[18] O.A. Bin-Dahman, T.A. Saleh, Synthesis of polyamide grafted on biosupport as polymeric adsorbents for the removal of dye and metal ions, Biomass Convers. Biorefinery (2022) 1–14.
[19] F.A. Ngwabebhoh, A. Erdem, U. Yildiz, Synergistic removal of Cu (II) and nitrazine yellow dye using an eco-friendly chitosan-montmorillonite hydrogel: optimization by response surface methodology, J. Appl. Polym. Sci. 133 (29) (2016).
[20] K.H. Prashanth, R.N. Tharanathan, Chitin/chitosan: modifications and their unlimited application potential—an overview, Trends Food Sci. Technol. 18 (3) (2007) 117–131.
[21] H. Javadian, M. Ruiz, T.A. Saleh, A.M. Sastre, Ca-alginate/carboxymethyl chitosan/Ni0. 2Zn0. 2Fe2. 6O4 magnetic bionanocomposite: synthesis, characterization and application for single adsorption of Nd+ 3, Tb+ 3, and Dy+ 3 rare earth elements from aqueous media, J. Mol. Liq. 306 (2020) 112760.
[22] T.A. Saleh, A. Sarı, M. Tuzen, Chitosan-modified vermiculite for as (III) adsorption from aqueous solution: equilibrium, thermodynamic and kinetic studies, J. Mol. Liq. 219 (2016) 937–945.
[23] L. Zhang, Y. Zeng, Z. Cheng, Removal of heavy metal ions using chitosan and modified chitosan: a review, J. Mol. Liq. 214 (2016) 175–191.
[24] S. Begum, N.Y. Yuhana, N.M. Saleh, N.H.N. Kamarudin, A.B. Sulong, Review of chitosan composite as a heavy metal adsorbent: material preparation and properties, Carbohydr. Polym. 259 (2021), 117613.
[25] R.I. Barnhisel, P.M. Bertsch, Chlorites and hydroxy-interlayered vermiculite and smectite, Miner. Soil Environ. 1 (1989) 729–788.
[26] O. Abollino, A. Giacomino, M. Malandrino, E. Mentasti, Interaction of metal ions with montmorillonite and vermiculite, Appl. Clay Sci. 38 (3–4) (2008) 227–236.
[27] T.A. Saleh, M. Tuzen, A. Sarı, Magnetic vermiculite-modified by poly (trimesoyl chloride-melamine) as a sorbent for enhanced removal of bisphenol A, J.Environ. Chem. Eng. 7 (6) (2019), 103436.
[28] A.A. Basaleh, M.H. Al-Malack, T.A. Saleh, Methylene blue removal using polyamide-vermiculite nanocomposites: kinetics, equilibrium and thermodynamic study, J. Environ. Chem. Eng. 7 (3) (2019), 103107.
[29] F.G. Calvo-Flores, J.A. Dobado, Lignin as renewable raw material, ChemSusChem 3 (11) (2010) 1227–1235.
[30] G. Zhang, Y. Wen, Z. Liu, S. Zhang, G. Li, Acid-catalyzed hydrolysis of conifer lignosulfonate in black liquor for the production of value-added chemicals, Appl. Catal. A Gen. 542 (2017) 1–9.
[31] Z.M. Şenol, A chitosan-based composite for adsorption of uranyl ions; mechanism, isothems, kinetics and thermodynamics, Int. J. Biol. Macromol. 183 (2021) 1640–1648.
[32] I. Langmuir, The adsorption of gases on plane surfaces of glass, mica and platinum, J. Am. Chem. Soc. 40 (9) (1918) 1361–1403.
[33] H.M.F. Freundlich, Über die adsorption in lösungen, Z. Physik. Chem. (Leipzig) 57A (1906) 385–470.
[34] A.O. Dada, A.P. Olalekan, A.M. Olatunya, O.J.I.J.C. Dada, Langmuir, freundlich, temkin and dubinin-radushkevich isotherms studies of equilibrium sorption of Zn2 + unto phosphoric acid modified rice husk, IOSR J. Appl. Chem. 3 (1) (2012) 38–45.
[35] S. Lagergren, Zur theorie der sogenannten adsorption geloster stoffe. Kungliga svenska vetenskapsakademiens, Handlingar 24 (1898) 1–39.
[36] Y.S. Ho, G. McKay, The kinetics of sorption of divalent metal ions onto sphagnum moss peat, Water Res. 34 (3) (2000) 735–742.
[37] F.C. Wu, R.L. Tseng, R.S. Juang, Initial behavior of intraparticle diffusion model used in the description of adsorption kinetics, Chem. Eng. J. 153 (1–3) (2009) 1–8.
[38] Z.M. Şenol, S. Şimşek, A. Özer, D. Şenol Arslan, Synthesis and characterization of chitosan–vermiculite composite beads for removal of uranyl ions: isotherm, kinetics and thermodynamics studies, J. Radioanal. Nucl. Chem. 327 (1) (2021) 159–173.
[39] Z.M. Şenol, N. Gürsoy, S. Şimşek, A. Özer, N. Karakuş, Removal of food dyes from aqueous solution by chitosan-vermiculite beads, Int. J. Biol. Macromol. 148 (2020) 635–646.
[40] N. Prakash, M. Soundarrajan, S. Arungalai Vendan, P.N. Sudha, N.G. Renganathan, Contemplating the feasibility of vermiculate blended chitosan for heavy metal removal from simulated industrial wastewater, Appl. Water Sci. 7 (8) (2017) 4207–4218.
[41] M.K. Sureshkumar, D. Das, M.B. Mallia, P.C. Gupta, Adsorption of uranium from aqueous solution using chitosan-tripolyphosphate (CTPP) beads, J. Hazard. Mater. 184 (1–3) (2010) 65–72.
[42] M. Sprynskyy, I. Kovalchuk, B. Buszewski, The separation of uranium ions by natural and modified diatomite from aqueous solution, J. Hazard. Mater. 181 (1–3) (2010) 700–707.
[43] L.H. Jones, R.A. Penneman, Infrared spectra and structure of uranyl and transuranium (V) and (VI) ions in aqueous perchloric acid solution, J. Chem. Phys. 21 (3) (1953) 542–544.
[44] P. Ilaiyaraja, A.K.S. Deb, K. Sivasubramanian, D. Ponraju, B. Venkatraman, Adsorption of uranium from aqueous solution by PAMAM dendron functionalized styrene divinylbenzene, J. Hazard. Mater. 250 (2013) 155–166.
[45] Z. Kılıç, O. Atakol, S. Aras, D. Cansaran-Duman, P. Çelikkol, E. Emregul, Evaluation of different isotherm models, kinetic, thermodynamic, and copper biosorption efficiency of Lobaria pulmonaria (L.) Hoffm, J. Air Waste Manag. Assoc. 64 (1) (2014) 115–123.
[46] W.W. Ngah, L.C. Teong, M.M. Hanafiah, Adsorption of dyes and heavy metal ions by chitosan composites: a review, Carbohydr. Polym. 83 (4) (2011) 1446–1456.
[47] C. Lee, W. Yang, R.G. Parr, Development of the Colle-Salvetti correlation-energy formula into a functional of the electron density, Phys. Rev. B 37 (1988) 785.
[48] A.D. Becke, Density-functional thermochemistry. III. The role of exact exchange, J. Chem. Phys. 98 (1993) 5648.
[49] M.M. Francl, W.J. Petro, W.J. Hehre, J.S. Binkley, M.S. Gordon, D.J. De Frees, J. A. Pople, Self-consistent molecular orbital methods. XXIII. A polarization-type basis set for second-row elements, J. Chem. Phys. 77 (1982) 3654.
[50] S. Grimme, J. Antony, S. Ehrlich, H. Krieg, A consistent and accurate ab initio parametrization of density functional dispersion correction (DFT-D) for the 94 elements H-pu, J. Chem. Phys. 132 (2010), 154104.
[51] L.-P. Wang, C. Song, Geometry optimization made simple with translation and rotation coordinates, J. Chem. Phys. 144 (2016), 214108.
[52] I.S. Ufimtsev, T.J. Martínez, Quantum chemistry on graphical processing units. 3 analytical energy gradients and first principles molecular dynamics, J. Chem. Theory Comput. 5 (2009) 2619.
[53] Jmol: an open-source Java viewer for chemical structures in 3D. http://www.jmol.org/.
[54] U. Hohm, Is there a minimum polarizability principle in chemical reactions? J. Phys. Chem. A 104 (36) (2000) 8418–8423.
[55] A.A. Al-Saadi, T.A. Saleh, V.K. Gupta, Spectroscopic and computational evaluation of cadmium adsorption using activated carbon produced from rubber tires, J. Mol. Liq. 188 (2013) 136–142.
[56] S. Şimşek, S. Kaya, Z.M. Şenol, H.İ. Ulusoy, K.P. Katin, A. Özer, N. Altunay, A. Brahmia, Theoretical and experimental insights about the adsorption of uranyl ion on a new designed vermiculite-polymer composite, J. Mol. Liquids 352 (2022), 118727.
[57] G. Wang, J. Liu, X. Wang, Z. Xie, N. Deng, Adsorption of uranium (VI) from aqueous solution onto cross-linked chitosan, J. Hazard. Mater. 168 (2–3) (2009) 1053–1058.
[58] A. Yang, P. Yang, C.P. Huang, Preparation of graphene oxide–chitosan composite and adsorption performance for uranium, J. Radioanal. Nuclear Chem. 313 (2) (2017) 371–378.
[59] T.S. Anirudhan, G.S. Lekshmi, F. Shainy, Synthesis and characterization of amidoxime modified chitosan/bentonite composite for the adsorptive removal and recovery of uranium from seawater, J. Colloid Interface Sci. 534 (2019) 248–261.
[60] D. Pan, Q. Fan, F. Fan, Y. Tang, Y. Zhang, W. Wu, Removal of uranium contaminant from aqueous solution by chitosan@ attapulgite composite, Sep. Purif. Technol. 177 (2017) 86–93.
[61] Z. Sun, D. Chen, B. Chen, L. Kong, M. Su, Enhanced uranium (VI) adsorption by chitosan modified phosphate rock, Colloids Surf. A Physicochem. Eng. Asp. 547 (2018) 141–147.
[62] J. Xu, M. Chen, C. Zhang, Z. Yi, Adsorption of uranium (VI) from aqueous solution by diethylenetriamine-functionalized magnetic chitosan, J. Radioanal. Nucl. Chem. 298 (2) (2013) 1375–1383.